ADVANCES IN ATMOSPHERIC SCIENCES, VOL. 31, JANUARY 2014, 179–187

Effects of a Remotely Sensed Land Cover Dataset with High Spatial Resolution on the Simulation of Secondary Air Pollutants over China Using the Nested-grid GEOS-Chem Chemical Transport Model

LI Mingwei[1,2], WANG Yuxuan*[1], and JU Weimin[3]

[1]*Ministry of Education Key Laboratory for Earth System Modeling, Center for Earth System Science, Institute for Global Change Studies, Tsinghua University, Beijing* 100084

[2]*School of Environment, Tsinghua University, Beijing* 100084

[3]*International Institute for Earth System Science, Nanjing University, Nanjing* 210093

(Received 19 November 2012; revised 10 March 2013; accepted 26 March 2013)

ABSTRACT

A number of remotely sensed land cover datasets with spatial resolutions $\leqslant$ 1 km have recently become available or are in the process of being mapped. The application of these higher resolution and more up-to-date land cover datasets in chemical transport models (CTMs) is expected to improve the simulation of dry deposition and biogenic emissions of non-methane volatile organic compounds (NMVOCs), which affect ozone and other secondary air pollutants. In the present study, we updated the land cover dataset in the nested-grid GEOS-Chem CTM with the 1 km resolution GLC2000 land cover map and examined the resulting changes in the simulation of surface ozone and sulfate over China in July 2007. Through affecting the dry deposition velocities of ozone and its precursors, using GLC2000 in the dry deposition module can decrease the simulated surface ozone by 3% (up to 6 ppb) over China. Simulated surface sulfate shows an increase of 3% in northwestern China and a decrease of 1% in northern China. Applying GLC2000 in the biogenic emissions of the NMVOC module can lead to a 0.5–4.5 ppb increase in simulated surface ozone over East China, mainly driven by the larger coverage of broadleaf trees in East China in the GLC2000 dataset. Our study quantifies the large sensitivity to land cover datasets with different spatial resolutions and time periods of simulated secondary air pollutants over China, supporting ongoing research efforts to produce high resolution and dynamically updated land cover datasets over China, as well as for the globe.

Key words: land cover, dry deposition, biogenic emissions, ozone, sulfate

Citation: Li, M. W., Y. X. Wang, and W. M. Ju, 2014: Effects of a remotely sensed land cover dataset with higher spatial resolution on secondary air pollutants simulation over China using the nested-grid GEOS-Chem chemical transport model. *Adv. Atmos. Sci.*, **31**(1), 179–187, doi: 10.1007/s00376-013-2290-1.

1. Introduction

Land cover type affects the dry deposition of gases and aerosols and natural emissions of some chemically active species. Forests provide a greater surface area for dry deposition of air pollutants such as ozone, aerosols and their precursors, than bare land (Wesely, 1989; Zhang et al., 2001). Non-methane volatile organic compounds (NMVOCs) including isoprene, monoterpenes, methyl butenol and other VOCs, emitted from certain vegetation species are important precursors for both tropospheric ozone (Wang et al., 1998) and secondary organic aerosol (SOA) (Liao et al., 2007). Nitrogen oxides (NO_x) emitted by soil microbes are also an important precursor for tropospheric ozone (Wang et al., 1998). Therefore, land cover mapping provides fundamental data for chemical transport models (CTMs).

Land cover maps commonly used in global and regional CTMs are typically derived from ecosystem inventories (e.g., Olson, 1992) or remote sensing studies (e.g., Friedl et al., 2002) with spatial resolutions $\geqslant$ 1 km. These datasets utilize different classification schemes, which are generally not the same as those required by contemporary CTMs, and hence need to be reclassified before applied in such models. For a given grid in a CTM, fractional vegetation cover and density [expressed as Leaf Area Index (LAI)] are needed in order to reflect the seasonal variation of land cover. As the LAI retrieval algorithm from satellite imagery is dependent on land cover (Liu et al., 2007), the land cover and LAI datasets used in CTMs should be consistent with each other.

There are several limitations of land cover datasets commonly used in CTMs. First, although the spatial resolutions of these datasets are generally finer than those of CTMs (tens to hundreds of kilometers), CTMs typically account for sev-

* Corresponding author: WANG Yuxuan
E-mail: yxw@tsinghua.edu.cn

eral land cover types and their corresponding percentages within each grid. Therefore, over regions with mixed types of land cover, higher resolution land cover datasets provide a more accurate representation of the dominant land type or mosaic patterns in CTMs. Second, global land cover is dynamic, but many CTMs tend to use land type datasets that represent the situation in the 1990s (e.g., Olson, 1992; Friedl et al., 2002), which are of course outdated and cannot capture the rapid change in land cover that has occurred in recent years, including urbanization, deforestation and reforestation. Recently, a number of global land cover maps with higher degrees of spatial resolution have been derived from different satellite sensors and made available to the community, including GLC2000 (1 km resolution) (Bartholomé and Belward, 2005), MODIS v5 (500 m resolution) (Friedl et al., 2010), and GlobCover v2.2 (300 m resolution) (Arino et al., 2008). There is currently an effort in China to develop a 30 m global land cover dataset (Chen et al., 2011).

Such higher resolution and more up-to-date land cover datasets are expected to improve the simulation of dry deposition and biogenic emissions of NMVOCs that affect ozone and other secondary air pollutants. Fu and Liao (2012) updated the land cover and LAI data in the GEOS-Chem model with MODIS v5 datasets and found that the interannual variations in biogenic emissions of VOCs (volatile organic compounds) alone can lead to 2%–5% differences in simulated ozone and SOA in summer over China. In this paper, we report on sensitivity simulations to investigate the effects of a remotely sensed land cover dataset at 1 km resolution (GLC2000) on the simulated surface concentrations of secondary air pollutants over China using the nested-grid GEOS-Chem model. We focus on surface ozone and sulfate since they are important secondary pollutants that have great implications for air quality and climate change.

2. Data and method

To quantify the effects of higher resolution and more up-to-date land cover datasets on surface ozone and sulfate simulated by the nested-grid GEOS-Chem model over China, we conducted a standard simulation and two sensitivity simulations with GLC2000 land cover datasets to examine the effects on dry deposition and the biogenic emissions of NMVOCs separately. As the GEOS-Chem model is an offline CTM driven by assimilated meteorology, we do not account for the effects of land cover change on meteorological fields, which in turn may affect surface ozone and sulfate.

2.1. *The GEOS-Chem model*

GEOS-Chem (http://acmg.seas.harvard.edu/geos) is a global 3D CTM driven by Goddard Earth Observing System (GEOS) assimilated meteorology from the National Aeronautics and Space Administration (NASA) Global Modeling and Assimilation Office (GMAO). The GEOS-Chem model includes a detailed and fully coupled tropospheric O_3–NO_x–hydrocarbon–aerosol simulation. The model version used in this study was v9-01-01. The nested-grid GEOS-Chem model was developed by Wang et al. (2004) and Chen et al. (2009). The structure of the nested-grid model involves a window with a horizontal resolution of $0.5^\circ \times 0.667^\circ$ (lat $\times$lon, hereafter) embedded in a low-resolution ($4^\circ \times 5^\circ$) global background. The nested domain is set at 70°–150°E and 11°S–55°N and includes all of China, its neighboring countries, and a significant portion of the northwestern Pacific Ocean.

The dry deposition process in GEOS-Chem is based on a resistance-in-series approach (Wesely, 1989) with a number of improvements, including the explicit dependence of canopy stomatal resistance on LAI (Gao and Wesely, 1995). The dry deposition velocities are dependent on the species properties, land cover type, LAI and meteorological conditions. The dry deposition module in v9-01-01 uses the Olson land map (Olson, 1992; hereafter referred to as OL1992) with a native spatial resolution of ~ 50 km. This map specifies 74 different land types, which are reclassified in the model to 11 types for gas dry deposition and 15 types for aerosol dry deposition (Table 1). When there are several Olson land types in a model grid of $0.5^\circ \times 0.667^\circ$, their corresponding fractions are considered.

Table 1. Land type classes for gas/aerosol dry deposition and biogenic emissions of VOCs in the GEOS-Chem model.

Number	Gas dry deposition	Number	Aerosol dry deposition	Number	MEGAN
1	Amazon forest	1	Evergreen broadleaf trees	1	Broadleaf trees
2	Deciduous forest	2	Deciduous broadleaf trees	2	Fineleaf trees
3	Coniferous forest	3	Evergreen needleleaf trees	3	Shrubs
4	Wetland	4	Deciduous needleleaf trees	4	Grass and other
5	Shrub/grassland	5	Mixed broadleaf and needleleaf trees	5	Crops
6	Agricultural land	6	Wet land with plants		
7	Tundra	7	Shrubs and interrupted woodlands		
8	Desert	8	Grass		
9	Water	9	Crops and mixed farming		
10	Snow/Ice	10	Desert		
11	Urban	11	Tundra		
		12	Inland Water		
		13	Ocean		
		14	Ice cap and glacier		
		15	Urban		

The biogenic emissions of NMVOCs in GEOS-Chem v9-01-01 adopts the MEGAN 2.1 scheme developed by Guenther et al. (2006). The emission flux for each NMVOC species in a grid box is a function of the baseline emission (in mg C m^{-2} h^{-1}), which is solely dependent on the plant functional type (PFT) and the emission activity factors related to LAI, temperature and solar radiation. The MEGAN 2.1 scheme specifies five different PFTs (Table 1) and each PFT has a constant baseline emission (in mg C m^{-2} h^{-1}). The MEGAN 2.1 PFT database combines the MODIS3 database and quantitative tree inventories based on ground observations where available (e.g., Kinnee et al., 1997) with a spatial resolution of $\sim$ 1 km. In each grid box, PFTs and their corresponding areal fractional coverage are given. The gridded monthly-mean LAI over 2000–08 in v9-01-01 is derived from a MODIS product of $\sim$ 1 km resolution (Myneni et al., 2002, 2007). In the MEGAN scheme, the weighted LAI (LAIv) is used and calculated in each grid by: LAIv = LAI/f, where f is the total fraction of all PFTs in a grid box. Table 2 summarizes the land cover datasets used in the dry deposition and MEGAN scheme of the GEOS-Chem standard simulation.

2.2. *Sensitivity simulations*

In the sensitivity simulations we adopted the 1-km resolution Global Land Cover 2000 (GLC2000) land cover dataset in GEOS-Chem's dry deposition and MEGAN schemes. The GLC2000 land cover dataset was generated from daily 1 km SPOT4-VEGETATION data from November 1999 to December 2000 (Bartholomé and Belward, 2005). It combined 19 regional products conducted separately by expert groups employing different classification procedures. Previous studies (Herold et al., 2008; Poulter et al., 2011) have suggested that the GLC2000 dataset and other existing land cover maps (e.g., MODIS v5 and GlobCover v2.2) have large spatial disagreement in heterogeneous landscapes characterized by a mosaic of trees, shrubs, grass and crops.

Table 2. The land cover datasets used in the standard and sensitivity simulations of the present study.

Data type	Name	Time period	Spatial resolution	Base data	Number of classes
Standard simulation					
Land cover	OL1992	before 1992	$\sim$ 50 km	Inventory	74
Land cover	MODIS	2001	$\sim$ 1 km	MODIS3, inventory	17
LAI	MODIS-based	2000–08, monthly	$\sim$ 1 km	MODIS	
Sensitivity simulation					
Land cover	GLC2000	2000	$\sim$ 1 km	SPOT-4	22
LAI	GLC2000-based	2000–10, 8 days	$\sim$ 500 m	MODIS, GLC2000	

Table 3. The GLC2000 classification scheme and reclassification for the GEOS-Chem model in Table 1. For each land type in the GLC 2000, the corresponding land type classes in the GEOS-Chem model and their percentages are given.

Number	GLC2000	Land type classes in Table 1 and their percentages		
		Gas dry deposition	Aerosol dry deposition	MEGAN
1	Tree cover, broadleaved, evergreen	1; 100%	1; 100%	1; 100%
2	Tree cover, broadleaved, deciduous, closed	2; 100%	2; 100%	1; 100%
3	Tree cover, broadleaved, deciduous, open	2; 100%	2; 100%	1; 100%
4	Tree cover, needle-leaved, evergreen	3; 100%	3; 100%	2; 100%
5	Tree cover, needle-leaved, deciduous	3; 100%	4; 100%	2; 100%
6	Tree cover, mixed leaf type	2, 3; 50%	5; 100%	1, 2; 50%
7	Tree cover, regularly flooded, fresh water (& brackish)	4; 100%	6; 100%	1, 2; 50%
8	Tree cover, regularly flooded, saline water	4; 100%	6; 100%	1, 2; 50%
9	Mosaic: Tree cover/other natural vegetation	2, 3, 5; 33%	5, 7, 8; 33%	1, 2, 3, 4; 25%
10	Tree cover, burnt	5; 100%	7; 100%	0
11	Shrub cover, closed-open, evergreen	5; 100%	7; 100%	3; 100%
12	Shrub cover, closed-open, deciduous	5; 100%	7; 100%	3; 100%
13	Herbaceous cover, closed-open	5; 100%	8; 100%	4; 100%
14	Sparse herbaceous or sparse shrub cover	5; 50%	7, 8; 25%	3, 4; 25%
15	Regularly flooded shrub and/or herbaceous cover	4; 100%	6; 100%	3, 4; 50%
16	Cultivated and managed areas	6; 100%	9; 100%	5; 100%
17	Mosaic: cropland/tree cover/other natural vegetation	2, 3, 5, 6; 25%	5, 7, 8, 9; 25%	1, 2, 3, 4, 5; 20%
18	Mosaic: cropland/shrub or grass cover	5, 6; 50%	7, 8, 9; 33%	3, 4, 5; 33%
19	Bare areas	8; 100%	10; 100%	0
20	Water bodies (natural & artificial)	9; 100%	13; 100%	0
21	Snow and ice (natural & artificial)	10; 100%	14; 100%	0
22	Artificial surfaces and associated areas	11; 100%	15; 100%	0

We reclassified the 22 categories of land cover in GLC2000 to land cover classes in GEOS-Chem (Table 3). For some categories, the reclassification was straightforward. For example, the category of "tree cover, broadleaved, deciduous, open" in GLC2000 was reclassified as "deciduous forest" in GEOS-Chem's dry deposition scheme for gases. For "mixed type" or "mosaic" categories in GLC2000, an equal probability was given for each land cover type contained in this category. For example, the "mosaic: tree cover/other natural vegetation" in GLC2000 was classified as 25% each for "broadleaf trees", "fineleaf trees", "shrubs" and "grass" in the MEGAN scheme. The GLC2000 dataset does not separate "desert" and "tundra", instead classifying them as "bare areas". We reclassified "bare areas" as "desert" in the GEOS-Chem dry deposition scheme. We used the LAI data retrieved from GLC2000, MOD 09A1 and MCD 43A1 data with a temporal and spatial resolution of 8 days and 500 m over China (Liu et al., 2012). This LAI dataset has been validated based on six typical forests in China, with all accuracies found to be above 70% (Liu et al., 2012). Table 2 summarizes the land cover and LAI datasets used in the sensitivity simulations.

We performed two sensitivity simulations, one for the dry deposition process and the other for the biogenic emissions of NMVOCs. Both simulations were conducted for the most vegetated month (July) in 2007, when the two processes were expected to have the largest influence on the budget of ozone and sulfate. Although hundreds of biogenic NMVOCs have been identified, isoprene emissions dominate annual fluxes to the atmosphere (Guenther et al., 2006). Therefore, for simplicity, we only updated the baseline emissions of isoprene with the GLC2000 dataset.

3. Results and discussion

In this section, we analyze the differences between the standard and sensitivity simulations for the dry deposition process and the biogenic emissions of NMVOCs separately.

3.1. *Dry deposition*

As gas and aerosol dry deposition involves different types of land cover, we discuss the resulting difference in surface ozone and sulfate separately. The difference in surface ozone between the standard and sensitivity simulation ("sensitivity minus standard" hereafter) is determined by the difference in dry deposition velocities of both ozone and its precursors, such as NO_x and VOCs. Figure 1 shows the dominant land cover in each model grid ($0.5^\circ \times 0.667^\circ$) of the OL1992 and GLC2000 datasets over China for gas dry deposition. The main differences between the two datasets are in western and southern China. Figure 2 shows simulated surface NO_x (Fig. 2b), ozone dry deposition velocity (Fig. 2d), and surface ozone (Fig. 2f) in the standard simulation and the corresponding differences between the standard and sensitivity simulation in July 2007. With the use of GLC2000, the simulated monthly-mean surface NO_x and dry deposition velocity of ozone decreases by 9% and 4.5% respectively over China, while VOCs do not show significant changes. These effects in combination result in a 3% decrease of monthly-mean surface ozone over China (up to 6 ppb). We ran another simulation using the July 2008 meteorology and found that the sensitivity of ozone to meteorological fields is 0–10 ppb over China. Thus, the sensitivity to land cover of ozone is comparable with that to meteorological fields.

As shown in Fig. 2f, the resulting difference of surface ozone has large spatial variability. Therefore, we analyze the differences for three regions in China: western China (WC; 30°–45°N, 80°–100°E), Central China (CC; 30°–40°N, 100°–110°E) and southern China (SC; 22°–30°N, 104°–122°E). In WC, a large portion of "tundra" in the OL1992 dataset is classified as "shrub/grassland" in GLC2000. As a result, the NO_x dry deposition velocity increases by 4% for the sensitivity simulation in this region. However, the ozone dry deposition velocity does not show significant changes. As NO_x has a relatively low abundance in WC, the decrease of surface NO_x locally and at its upwind regions such as India

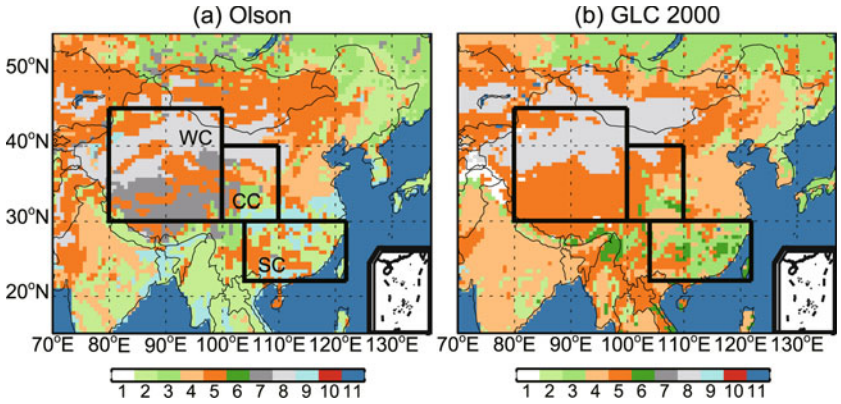

Fig. 1. The dominant land cover in each model grid ($0.5^\circ \times 0.667^\circ$) of (a) OL1992 and (b) GLC2000 over China for the classes of gas dry deposition. The black boxes indicate the definition of three regions in China (WC, CC and SC). Key: 1 Snow/ice; 2 Deciduous forest; 3 Coniferous forest; 4 Agricultural land; 5 Shrub/grassland; 6 Amazon forest; 7 Tundra; 8 Desert; 9 Wetland; 10 Urban; 11 Water.

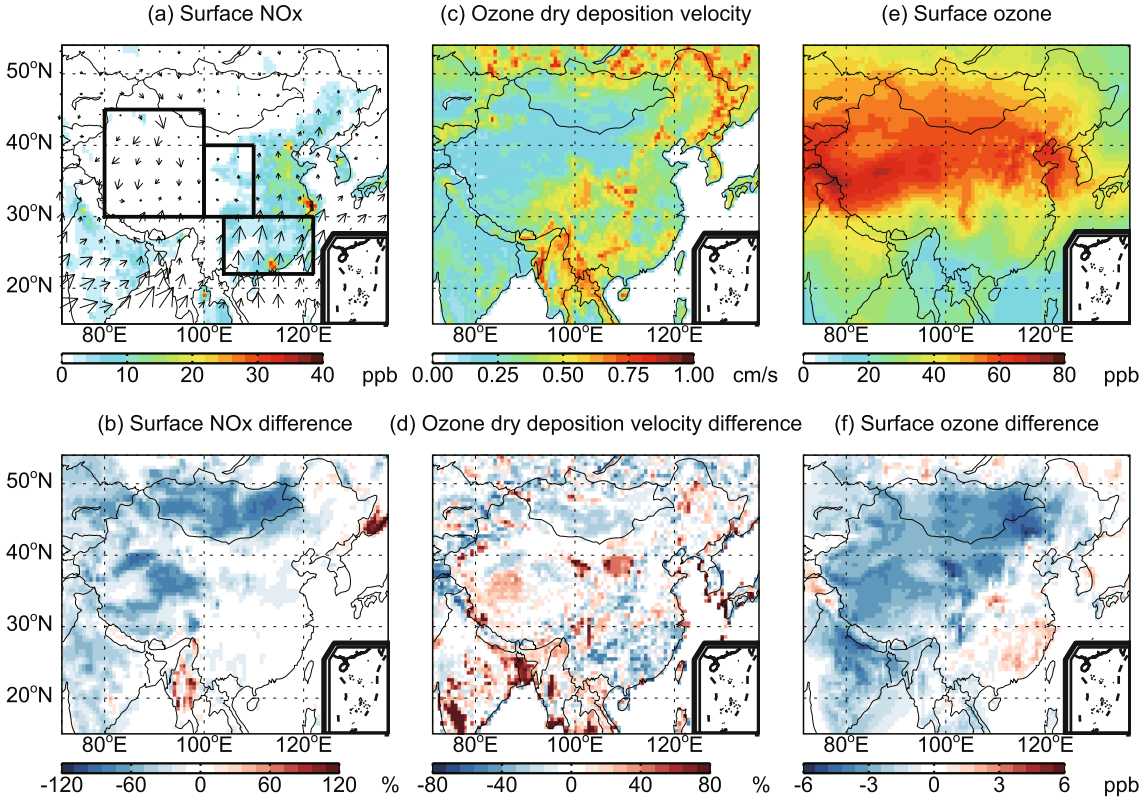

Fig. 2. Simulated (a) surface NO_x; (c) ozone dry deposition velocity; and (e) surface ozone in the standard simulation and (b, d, f) the corresponding differences between the standard and sensitivity simulation (sensitivity minus standard) in Jul 2007. Figure 2a also shows the monthly-mean surface wind fields in Jul 2007. The black boxes indicate the definition of three regions in China (WC, CC and SC).

(Fig. 2b) reduce the monthly-mean surface ozone by up to 4 ppb (5%). In SC and CC, where the surface NO_x does not show any apparent difference, the difference of surface ozone is determined by the change of ozone dry deposition velocity. In SC, most of the "deciduous forest" in the OL1992 dataset is classified as "coniferous forest" in GLC2000. As coniferous forest provides less dry deposition area than deciduous forest, the dry deposition velocities of ozone decrease by 18% in this region using GLC2000. As wet deposition of ozone precursors plays a more important role in July over SC, the 18% decrease of ozone dry deposition velocity over this region only increases the monthly-mean surface ozone by 1.2% (up to 2 ppb). In CC, some of the "tundra" and "desert" areas in the OL1992 dataset are detected as "shrub/grassland" in GLC2000. This leads to a 4% increase in the ozone dry deposition velocity. In response, a 5% decrease in the monthly-mean surface ozone is found and the maximal decrease can be up to 6 ppb in this region.

Figure 3 shows the dominant land cover in each model grid [0.5°(lat) × 0.667° (lon)] of the OL1992 and GLC2000 datasets over China for aerosol dry deposition. Figure 4 shows the simulated sulfate dry deposition velocity and surface sulfate in the standard simulation and the corresponding differences between the standard and sensitivity simulation in July 2007. In northwestern China (NWC; 35°–50°N, 80°–100°E), the dry deposition velocities of sulfate decrease by 15% with the use of GLC2000. This is largely driven by the replacement of "shrub" in the OL1992 dataset with "desert" in GLC2000. In response, the monthly-mean surface sulfate increases by 3% (up to 0.2 μg m^{-3}) in this region. In northern China (NC; 34°–42°N, 100°–122°E), the change of "desert" in the OL1992 dataset to "grass" in GLC2000 increases the dry deposition velocities of sulfate by 8%. Consequently, the monthly-mean surface sulfate decreases by 1% (up to 0.4 μg m^{-3}) in this region. We ran another simulation using the July 2008 meteorology and found that the sensitivity of sulfate to meteorological fields is 0–2 μg m^{-3}over China. Thus, the sensitivity of sulfate to land cover is comparable with that to meteorological fields.

3.2. *Biogenic emissions of NMVOCs*

Figure 5 shows the difference of PFTs and LAIv between MODIS and GLC2000 in July 2007 over China. The baseline emissions of isoprene vary significantly among different PFTs. Broadleaf trees and shrubs have the highest baseline emissions of 13.0 and 11.0 mg C m^{-2} h^{-1}, respectively, compared to needleleaf trees (2.0 mg C m^{-2} h^{-1}), grass and crops (0.4 mg C m^{-2} h^{-1}). Therefore, the differ-

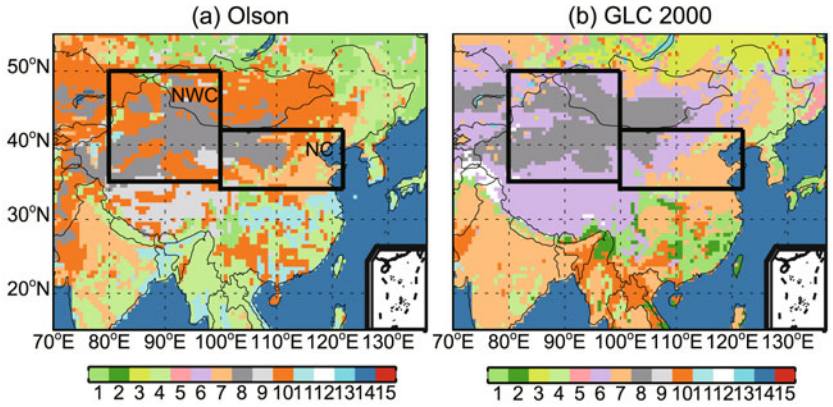

Fig. 3. The same as Fig. 1 but for aerosol dry deposition. The black boxes indicate the definition of two regions in China (NWC and NC). Key: 1 Evergreen needleleaf trees; 2 Evergreen broadleaf trees; 3 Deciduous needleleaf trees; 4 Deciduous broadleaf trees; 5 Mixed broadleaf and needleleaf trees; 6 Grass; 7 Crops and mixed farming; 8 Desert; 9 Tundra; 10 Shrubs and interrupted woodlands; 11 Wet land with plants; 12 Ice cap and glacier; 13 Inland water; 14 Ocean; 15 Urban.

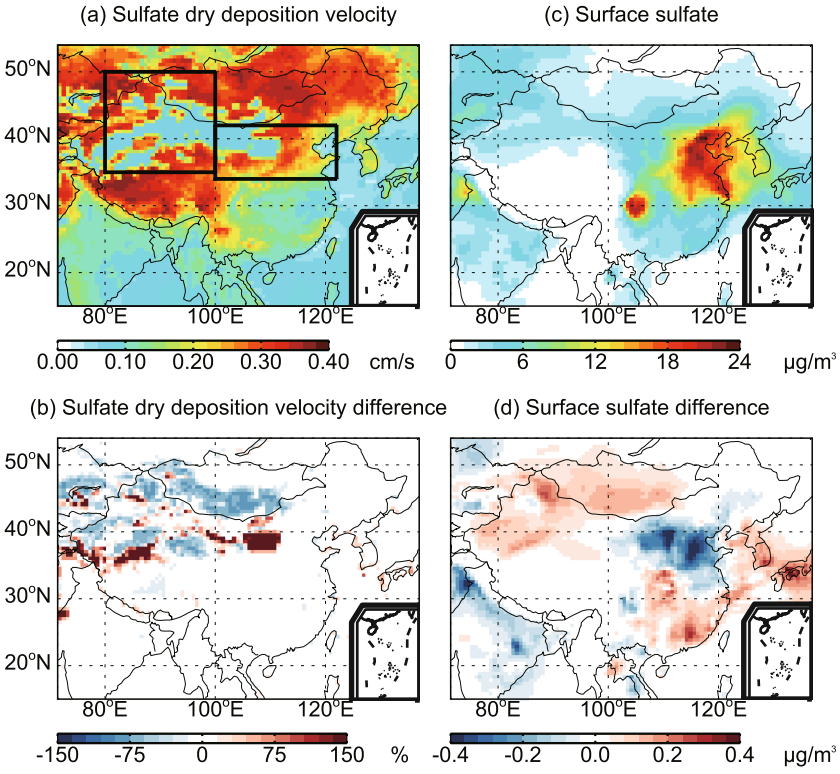

Fig. 4. Simulated (a) sulfate dry deposition velocity and (c) surface sulfate in the standard simulation and (b, d) the corresponding differences between the standard and sensitivity simulation (sensitivity minus standard) in Jul 2007. The black boxes indicate the definition of two regions in China (NWC and NC).

ence in broadleaf trees and shrubs between the two datasets dominates the difference in isoprene baseline emissions. Table 4 summaries the differences in areal fractional coverage of each PFT between MODIS and GLC2000. Over China, the GLC2000 dataset has a 5.8% larger areal coverage of broadleaf trees than the MODIS dataset, with the difference mainly in the southeast and northeast of China. On the contrary, the GLC2000 has a 5.3% smaller areal coverage of shrubs, mainly in the southwest of China. The MEGAN scheme requires LAIv for the simulation month, the previous month, and the next month to calculate the emission activity factors. The GLC2000-based LAIv during June–August

Table 4. The areal fractional coverage (%) of five PFTs and non-vegetated land for MODIS and GLC2000 land cover datasets over China.

PFT	MODIS (%)	GLC2000 (%)	Difference (%)
Broadleaf trees	3.3	9.1	5.8
Fineleaf trees	9.8	10.4	0.6
Shrubs	10.3	5	−5.3
Grass and other	14.9	28.2	13.3
Crops	15	17.1	2.1
Unvegetated land	46.7	30.2	−16.5

2007 is 28% larger than that in the standard simulation over China. Figure 5 shows that the spatial distribution of the difference in LAIv is mostly consistent with that in broadleaf trees.

The simulated isoprene emissions and surface ozone in the standard simulation and the corresponding differences between the standard and sensitivity simulation for July 2007 are presented in Fig. 6. Combining the differences in PFTs and LAIv, the isoprene emissions increase by 44% over China, with the changes mainly over the southeast and northeast of China. Higher isoprene emissions in the sensitivity simulation lead to a 0.5–4.5 ppb increase of surface ozone in East China, where NO_x has a relatively high abundance compared to VOCs. Figure 6a also shows the simulated monthly-mean surface wind fields in July 2007. Over East China, the increase in surface ozone happens downwind of the regions where isoprene emissions increase.

4. Conclusions

We performed two types of sensitivity simulations using the GLC2000 dataset to examine the impact of higher resolution and more up-to-date land cover on dry deposition and biogenic emissions of NMVOCs schemes in the GEOS-Chem model for July 2007. The differences in two important secondary air pollutants—ozone and sulfate —have been analyzed between the standard and sensitivity simulation. Using the GLC2000 dataset, the simulated surface ozone in July 2007 decreases by 5% (up to 4 ppb) in WC, mainly due to the decrease in surface NO_x. The 5% decrease (up to 6 ppb) in simulated surface ozone in CC and the 1.2% increase (up to 2 ppb) in SC result from the change in ozone dry deposition velocity. The surface sulfate in the sensitivity simulation shows an increase of 3% in NWC and a decrease of 1% in NC, which are due to the changes in dry deposition velocities of sulfate. We did not apply the GLC2000-based LAI datasets in the dry deposition module, which will reduce the sensitivity and needs further consideration. Using the GLC2000 dataset in

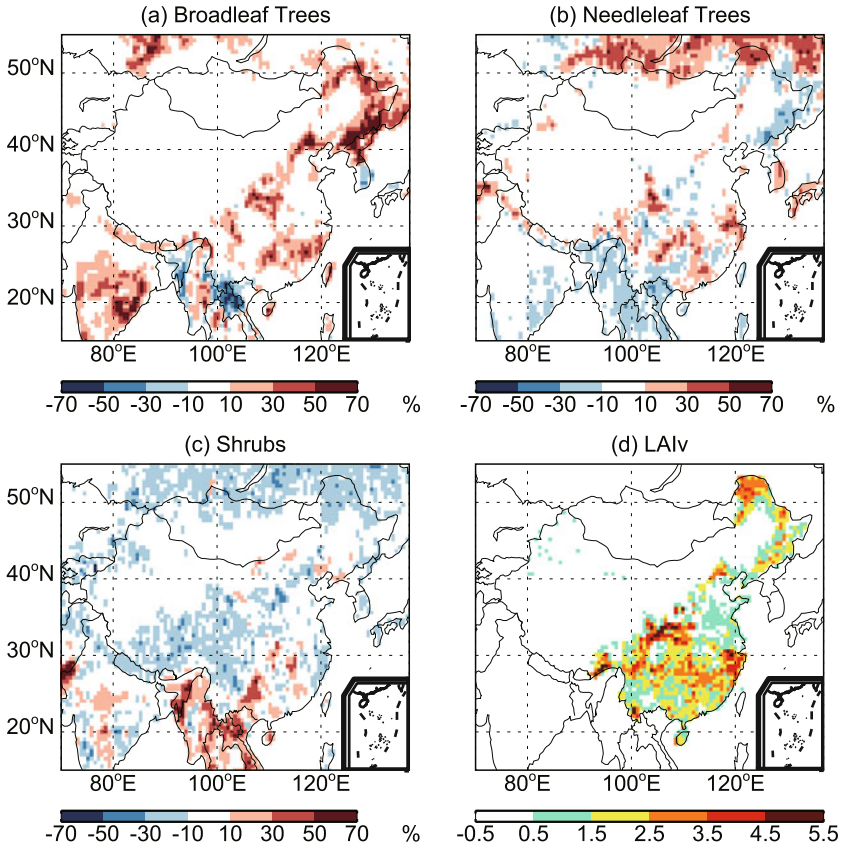

Fig. 5. Differences in areal fractional coverage of (a) broadleaf trees; (b) needleleaf trees; (c) shrubs; and (d) difference of mean LAIv for Jun–Aug 2007 between the MODIS and GLC2000 datasets (GLC2000 minus MODIS).

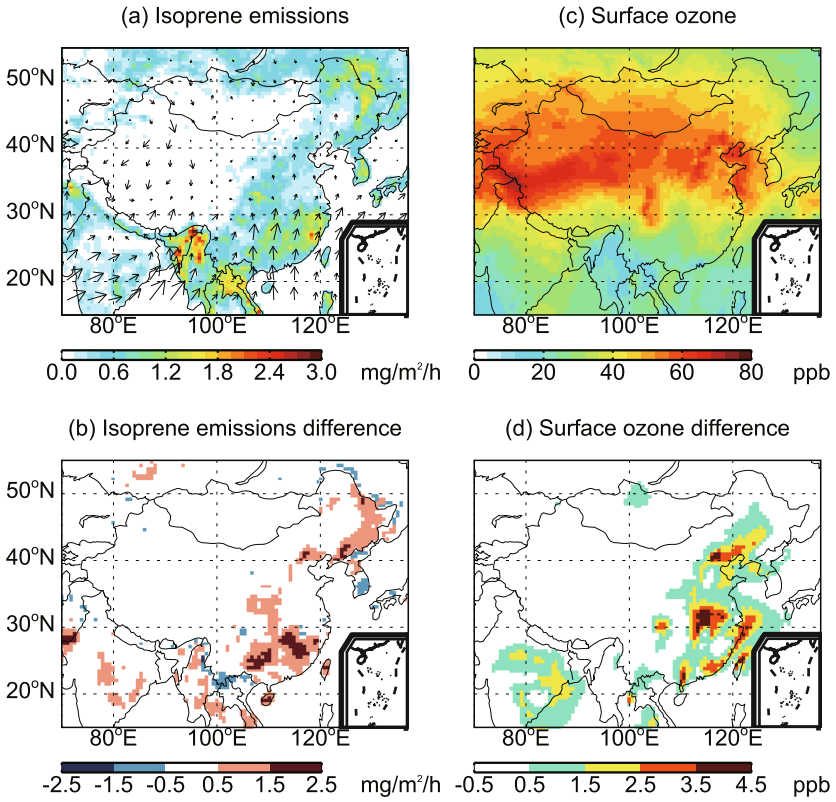

Fig. 6. Simulated (a) isoprene emissions and (c) surface ozone in the standard simulation and (b, d) the corresponding differences between the standard and sensitivity simulation (sensitivity minus standard) in Jul 2007. (a) also shows the monthly-mean surface wind fields in Jul 2007.

the biogenic emissions of the NMVOC module leads to an increase of simulated surface ozone by 0.5–4.5 ppb in the east of China, mainly due to the larger areal coverage of broadleaf trees in the southeast and northeast of China.

Our study has shown that the simulated secondary air pollutants by CTMs are sensitive to land cover datasets with different spatial resolutions and time periods. In addition to the two processes and the two secondary air pollutants considered in this study, the sensitivities of higher resolution land cover on dust emissions, soil NO_x emissions and SOA also deserve to be studied. A more important scientific question to be addressed in the future is how the land cover change in China over recent decades has impacted upon the concentration of ozone and aerosols.

Acknowledgements. This work was supported by the National High-Technology Research and Development Program of China (Grant No. 2009AA122005) and the Beijing Nova Program (Grant No. Z121109002512052). We thank Prof. Dylan MILLET (University of Minnesota) for help on the MEGAN scheme in GEOS-Chem.

REFERENCES

Arino, O., P. Bicheron, F. Achard, J. Latham, R. Witt, and J. L. Weber, 2008: GLOBCOVER The most detailed portrait of Earth. *ESA Bulletin-European Space Agency*, 24–31.

Bartholomé, E., and A. S. Belward, 2005: GLC2000: A new approach to global land cover mapping from earth observation data. *Int. J. Remote Sens.*, **26**, 1959–1977.

Chen, D., Y. Wang, M. B. McElroy, K. He, R. M. Yantosca, and P. Le Sager, 2009: Regional CO pollution and export in China simulated by the high-resolution nested-grid GEOS-Chem model. *Atmos. Chem. Phys.*, **9**, 3825–3839.

Chen, J., J. Chen, P. Gong, A. P. Liao, and C. Y. He, 2011: Higher resolution global land cover mapping. *Geomatics World*, **2**, 12–14.

Friedl, M. A., and Coauthors, 2002: Global land cover mapping from MODIS: Algorithms and early results. *Remote Sens. Environ.*, **83**, 287–302.

Friedl, M. A., D. Sulla-Menashe, B. Tan, A. Schneider, N. Ramankutty, A. Sibley, and X. Huang, 2010: MODIS collection 5 global land cover: Algorithm refinements and characterization of new datasets. *Remote Sens. Environ.*, **114**, 168–182.

Fu, Y., and H. Liao, 2012: Simulation of the interannual variations of biogenic emissions of volatile organic compounds in China: Impacts on tropospheric ozone and secondary organic aerosol. *Atmos. Environ.*, **59**, 170–185.

Gao, W., and M. L. Wesely, 1995: Modeling gaseous dry deposition over regional scales with satellite observations, 1. Model development. *Atmos. Environ.*, **29**, 727–737.

Guenther, A., T. Karl, P. Harley, C. Wiedinmyer, P. I. Palmer, and C. Geron, 2006: Estimates of global terrestrial isoprene emissions using MEGAN (Model of Emissions of Gases and

Aerosols from Nature). *Atmos. Chem. Phys.*, **6**, 3181–3210.

Herold, M., P. Mayaux, C. E. Woodcock, A. Baccini, and C. Schmullius, 2008: Some challenges in global land cover mapping: An assessment of agreement and accuracy in existing 1 km datasets. *Remote Sens. Environ.*, **112**, 2538–2556.

Kinnee, E., C. Geron, and T. Pierce, 1997: United States land use inventory for estimating biogenic ozone precursor emissions. *Ecological Applications*, **7**, 46–58.

Liao, H., D. K. Henze, J. H. Seinfeld, S. Wu, and L. J. Mickley, 2007: Biogenic secondary organic aerosol over the United States: Comparison of climatological simulations with observations. *J. Geophys. Res.*, **112**, D06201.

Liu, R., J. M. Chen, J. Liu, F. Deng, and R. Sun, 2007: Application of a new leaf area index algorithm to China's landmass using MODIS data for carbon cycle research. *Journal Environmental Management*, **3**, 649–658.

Liu, Y. B., W. M. Ju, J. M. Chen, G. L. Zhu, B. L. Xing, J. F. Zhu, and M. Z. He, 2012: Spatial and temporal variations of forest LAI in China during 2000–2010. *Chinese Science Bulletin*, **57**, 2846–2856.

Myneni, R. B., and Coauthors, 2002: Global products of vegetation leaf area and fraction absorbed PAR from year one of MODIS data. *Remote Sens. Environ.*, **83**, 214–231.

Myneni, R. B., and Coauthors, 2007: Large seasonal swings in leaf area of Amazon rainforests. *Proc. Natl. Acad. Sci.*, **104**, 4820–4823.

Olson, J., 1992: World ecosystems (WE1.4): Digital raster data on a 10 minute geographic 1080×2160 grid. Global Ecosytems Database, Version 1.0: Disc A. NOAA National Geophysical Data Center, Boulder, Colorado.

Poulter, B., P. Ciais, E. Hodson, H. Lischke, F. Maignan, S. Plummer, and N. E. Zimmermann, 2011: Plant functional type mapping for earth system models. *Geoscientific Model Development*, **4**, 993–1010.

Wang, Y., D. J. Jacob, and J. A. Logan, 1998: Global simulation of tropospheric O_3-NO_x-hydrocarbon chemistry: 1. Model formulation. *J. Geophys. Res.*, **103**, 10713–10725.

Wang, Y. X., M. B. McElroy, T. Wang, and P. I. Palmer, 2004: Asian emissions of CO and NO_x: Constraints from aircraft and Chinese station data. *J. Geophys. Res.*, **109**, D24304.

Wesely, M. L., 1989: Parameterization of surface resistance to gaseous dry deposition in regional-scale numerical models. *Atmos. Environ.*, **23**, 1293–1304.

Zhang, L., S. Gong, J. Padro, and L. Barrie, 2001: A size-segregated particle dry deposition scheme for an atmospheric aerosol module. *Atmos. Environ.*, **35**, 549–560.